Coverage-dependent adsorption superstructure transition of C_{60}/Cu(001)

Sheng-Syun Wong
Department of Physics, National Taiwan University, Taipei 106, Taiwan

Woei Wu Pai*
Center for Condensed Matter Sciences, National Taiwan University, Taipei 106, Taiwan

Chia-Hao Chen
National Synchrotron Radiation Research Center, Hsinchu 300, Taiwan

Minn-Tsong Lin†
Department of Physics, National Taiwan University, Taipei 106, Taiwan
and Institute of Atomic and Molecular Sciences, Academia Sinica, Taipei 106, Taiwan
(Received 4 April 2010; revised manuscript received 4 July 2010; published 24 September 2010)

We have investigated the growth and structure of a C_{60} monolayer film on Cu(001) with scanning tunneling microscopy at room temperature and 100 K. We discovered that the equilibrium adsorption structure of annealed C_{60} films depends sensitively on the initial deposition coverage; for a coverage of 0.5 monolayer C_{60} orders in an one-bright-and-one-dim (1B1D) row sequence along the [110] direction whereas for a coverage close to one monolayer C_{60} orders in a two-bright-and-one-dim (2B1D) sequence. At the transition region of the bright and dim row segments, C_{60} often appears "frizzy" at room temperature. This indicates that a C_{60} rotates and adopts molecular orientations with inequivalent symmetry. Upon annealing, the C_{60} film exhibits a high thermal stability before C_{60} fragmentation and desorption occur at ~880–960 K, depending on its adsorption superstructure. The duality of equilibrium superstructure in C_{60}/Cu(001) is unique among studied C_{60} monolayers on metals. We argue that different boundary energy of the 1B1D and 2B1D phases offers a plausible explanation on the observed tunability of superstructure versus coverage.

DOI: 10.1103/PhysRevB.82.125442 PACS number(s): 68.55.ap, 68.35.bp, 68.37.Ef, 68.35.Rh

Since the discovery of C_{60} buckminsterfullerene by Kroto *et al.* in 1985,[1] great efforts have been made to understand the physical and chemical properties of fullerene materials. In particular, the nucleation, growth, and structure of ultrathin C_{60} films on various surfaces draw significant attention in the past two decades.[2–9] A general picture emerged primarily from scanning tunneling microscopy (STM) studies is that a C_{60} film often adopts close-packed hexagonal or quasi-hexagonal structure, with a C_{60} nearest-neighbor (NN) distance at most slightly changed from the C_{60} bulk NN value of 10.0 Å. This is because the intermolecular van der Waals adsorbate-adsorbate interactions often dominate over the adsorbate-substrate interactions. The latter interaction plays a more subtle role; when a C_{60} molecule adsorbs on a preferred adsorption site, it can often lead to C_{60}-induced substrate reconstruction and result in a dimmer C_{60} appearance in STM.[10–17] Therefore, the often observed bright-and-dim-C_{60} superstructures in C_{60} films are a consequence of incommensurability between a close-packed C_{60} film and the substrate. For example, when a close-packed C_{60} film adsorbs on a substrate of different symmetry, e.g., Ag(001), it leads to incommensurability mostly in one direction only and forms a so-called "aperiodic incommensurate" phase[18] showing molecular contrast with merely short-range order. For another noble-metal Cu(001), a previous STM study[19] has revealed another superstructure with alternating sequence of "bright" and "dim" C_{60} rows. Here we report two classes of superstructure, one has a two-bright-and-one-dim (2B1D) sequence ordering along [110] and another has an one-bright-and-one-dim (1B1D) sequence instead. We discovered that these two types of ordering at equilibrium (after sufficient annealing) depend on the initial C_{60} surface coverage, e.g., for coverage of ~1 monolayer (ML) the preferred type is 2B1D and for lesser coverage (e.g., ~0.5 ML) the preferred type becomes 1B1D. This result is unexpected because C_{60} aggregates into close-packed islands. Therefore, although the overall surface coverage decreases, the local packing density inside a C_{60} island is not expected to change and one would not expect the superstructure to change. We shall argue that boundary energy of C_{60} islands plays a plausible role to "tune" the superstructure type as C_{60} coverage changes.

It must be noted that the 2B1D and 1B1D superstructures we studied are thermal equilibrium phases, rather than metastable disordered structure. Figure 1(a) is a room-temperature STM micrograph of a full C_{60} monolayer on Cu(001) post-annealed to 648 K. The 2B1D sequence is seen in the regime marked "2B1D." Ordered row sequence appears regularly after annealing to a temperature $(T_A) \geq 650$ K. This ordered phase appears to have a rather high thermal stability; we found that fragmentation and desorption became evident only when T_A exceeded 950 K. When the initial surface C_{60} coverage is 0.5 ML, the annealed (at 600 K) equilibrium superstructure changes from 2B1D to 1B1D. This is shown in Fig. 1(b). This phase has a lower thermal stability, with fragmentation and desorption at $T_A \geq 880$ K. We thus refer the equilibrium 2B1D (1B1D) superstructures as the ordered structures produced by annealing to $650(600) \leq T_A \leq 900(800)$ K. Furthermore, higher annealing temperatures lead two phases to better ordering.

We conducted measurements at a temperature (T_m) of 300

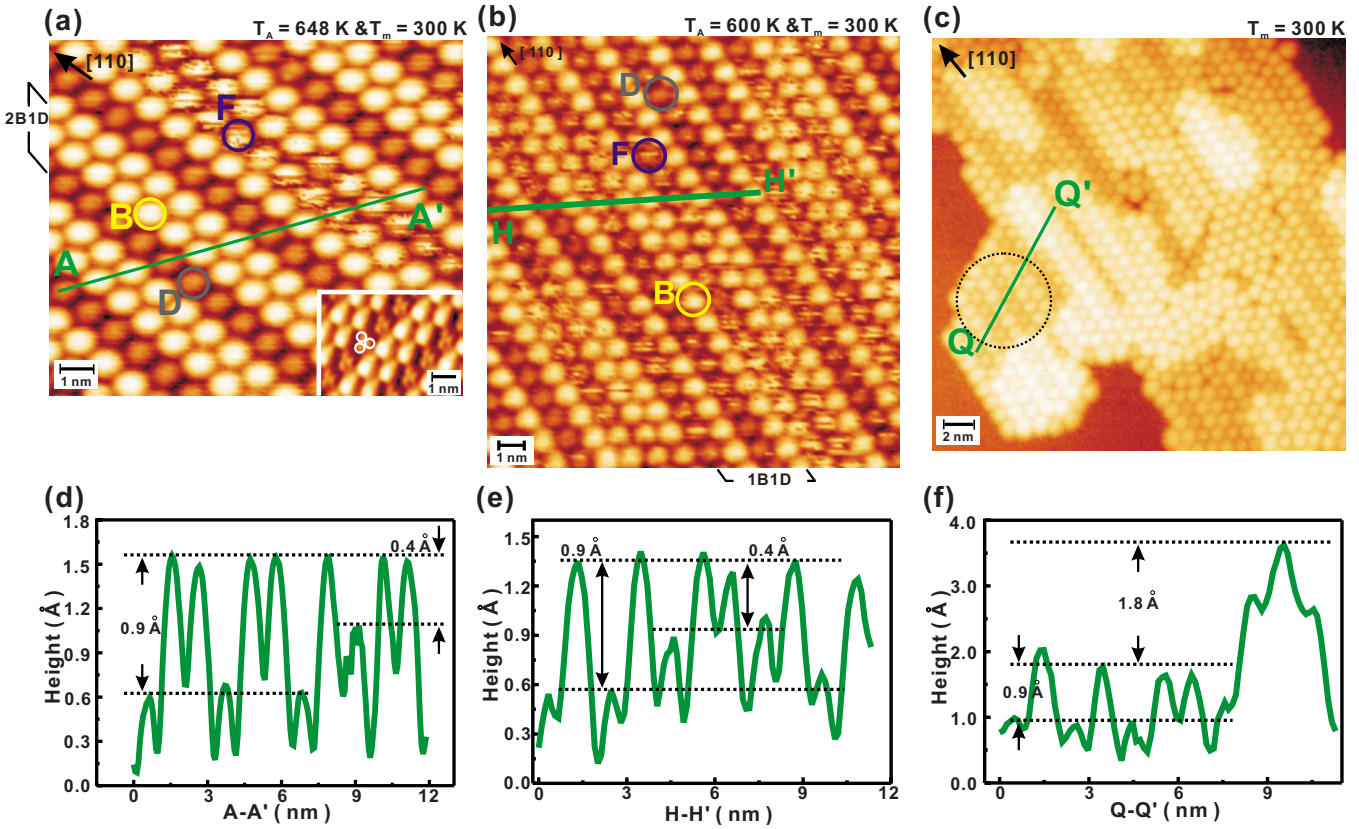

FIG. 1. (Color online) (a) and (b) are the STM images of full and half coverage after postannealing, respectively. All the STM images were taken at room temperature. The inset in (a) shows a higher resolution STM image. (c) is an STM image of 0.5 ML C_{60}/Cu(001) prepared and imaged at room temperature without postannealing. The molecular layer is obviously poorly ordered. Note some region (circled) already exhibits the 1B1D ordering. (d), (e), and (f) show the line profiles from (a), (b), and (c), respectively.

or 100 K. The experiments were conducted with a commercial Omicron variable-temperature scanning probe microscopy (SPM) and a room-temperature SPM housed in two separate home-built ultrahigh vacuum chambers with a base pressure $\sim 5 \times 10^{-11}$ Torr. The Cu(001) crystal was cleaned by repeated cycles of 2 KeV neon or argon sputtering and annealing to ~800 K for 30 min. The cleanness of surface was judged by atomically flat terraces with a nominal terrace width $\geq$100 nm and the lack of step bunches and step pinning contaminants. Powder C_{60} with purity higher than 99.9% was deposited from heated alumina crucibles with a nominal rate of 0.005 ML/s. The sample was held at room temperature during deposition. Well-ordered C_{60} (full or sub) monolayer films were prepared by subsequent annealing at proper T_A for 1 h. The sample temperature quoted in this work was calibrated against a dummy Cu sample with identical geometry and was estimated to be accurate to ± 10 K.

Figure 1(c) shows 0.5 ML C_{60} deposited on Cu(001) at room temperature without further thermal annealing. The molecular layer seems to comprise regions with different layer thickness. The ratio of bright C_{60} to dim C_{60} exceeds ~10, indicating that room-temperature deposition has not yet led to extensive interface reconstruction.[11,18] Therefore, the ordering of the C_{60} phase is very poor due to kinetic hindrance. The STM contour line depicted in Fig. 1(f) reveals not only the ~0.9 Å height difference between the bright and dim C_{60} but also the ~1.8 Å height of a Cu(001) single step. Similar disordered phase was also observed for unannealed 1 ML C_{60}.

The 2B1D structure of Fig. 1(a) has two orthogonal domains due to the square symmetry of the Cu(001) substrate. This superstructure is identical to what Abel *et al.*[19] reported in an earlier study. A high-resolution view [Fig. 1(a) lower right inset] reveals that the dim C_{60} (denoted as D-C_{60} hereafter) has a three-lobe intramolecular feature at room temperature. The three-lobe C_{60} shape is typical of the lowest unoccupied molecular orbital for a C_{60} adsorbed with its carbon hexagon facing up. The intramolecular feature of the bright C_{60} (denoted as C_{60}) cannot be resolved at room temperature, however. Recent low-temperature (~8 K) STM studies[20,21] have found at least five different C_{60} orientations on Cu(001), indicating that the C_{60} adsorption geometries in this system vary and are by no means uniform. The multitude of possible adsorption configurations will likely lead to C_{60} switching between orientations with nearly degenerate energy. Here we report a distinct type of C_{60} (denoted as ~10%) contrast in addition to the D-C_{60} and B-C_{60}. The F-C_{60} molecule has a frizzy appearance; this is typically interpreted in STM as dynamical switching of configuration (such as frizziness of step edges[22]). We may compare the C_{60}/Cu(001) and the C_{60}/Ag(100) system.[18,19] In C_{60}/Ag(100), three C_{60} contrast types (bright, dim, and medium) are static. The fluctuating contrast of F-C_{60} suggests that the superstructure may be prone to change, as discussed

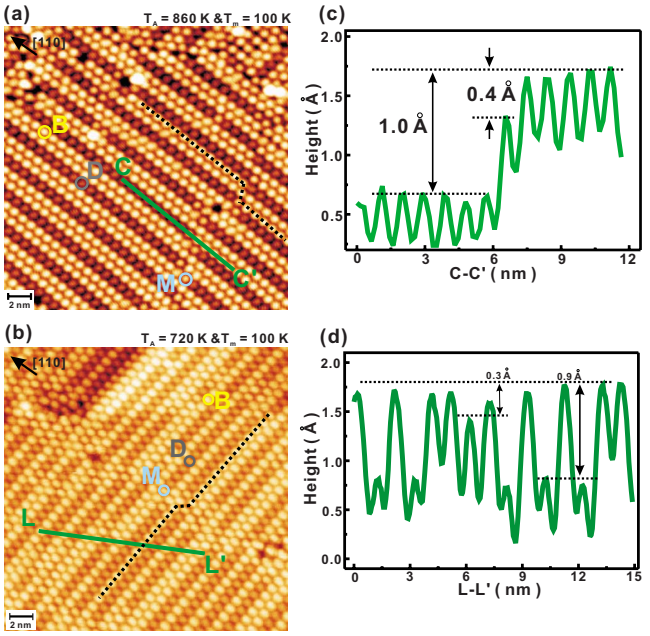

FIG. 2. (Color online) (a) and (b) are the 2B1D and 1B1D phases taken at 100 K. No frizzy C_{60} can be seen anymore, and a distinct C_{60} contrast (denoted as M) was observed. The dashed lines shown in (a) and (b) indicate that the 2B1D and 1B1D ordering often has offset. In (c) and (d), the line profiles from (a) and (b), respectively, are depicted.

in the 2B1D-1B1D transition later. The $C_{60}/Ag(100)$ molecules were most frequently observed in the regime when the contrast type along a C_{60} row changes from the B-C_{60} to the C_{60} or vice versa. We hereafter call such a transition region as "kink" sites. The presence of kinks is clearly due to the offset of the B-C_{60} and D-C_{60} rows along $[1\bar{1}0]$. For the 1B1D film as shown in Fig. 1(b), the 2B1D ordering was replaced by either 1B1D or some 1B1F (one-bright-and-one-frizzy) ordering. Similar to the 2B1D structure, the B-, D-, and F-C_{60} species are also present in 1B1D. Interestingly, the F-C_{60} species appears much more abundant in the 1B1D phase.

We first discuss the topographic contrast of the three C_{60} types in both the 2B1D and 1B1D phases, and at 300 and 100 K. Figure 1(d) shows a 2B1D line profile (AA′) of Fig. 1(a) at room temperature. The height difference between the B-C_{60} and D-C_{60} is $\sim 0.9 \pm 0.1$ Å. In addition, this difference is nearly bias independent from −2 to +2 V (not shown). The height difference between the F-C_{60} and B-C_{60} is $\sim 0.4 \pm 0.2$ Å. Figure 1(e) shows a 1B1D line profile (HH′) of Fig. 1(b). The height difference between the B-C_{60} and D-C_{60} is $\sim 0.9 \pm 0.1$ Å, and between the B-C_{60} and F-C_{60} is $\sim 0.4 \pm 0.1$ Å. Both are the same as those observed in the 2B1D phase [Fig. 1(d)]. Upon cooling, the overall 2B1D structure does not change but the F-C_{60} species disappears. Figure 2(a) is a 2B1D area taken at 100 K. No frizzy F-C_{60} can be seen anymore. Figure 2(c) shows the line profile (CC′) of Fig. 2(a). A distinct C_{60} contrast (denoted as M) was seen. Most of the M-C_{60} molecules locate at one or two kink sites. The height difference of the B-C_{60} and D-C_{60} remains at $\sim 0.9 \pm 0.1$ Å, same as that measured at room

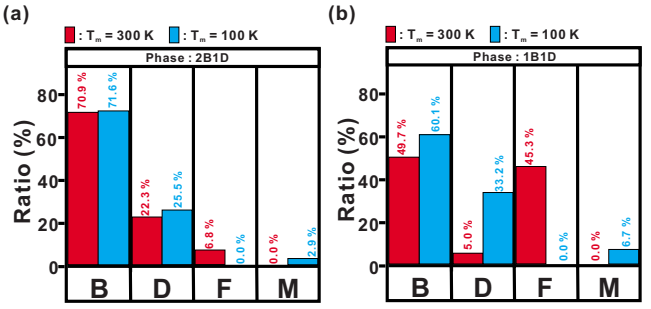

FIG. 3. (Color online) The ratios of B-, D-, F-, and M-C_{60} in the 2B1D and 1B1D phases at room temperature and 100 K are shown in (a) and (b), respectively.

temperature. The height difference of the B-C_{60} and M-C_{60} is $\sim 0.4 \pm 0.1$ Å. While this value is similar to that of the B-C_{60} and F-C_{60}, only a small fraction of room temperature F-C_{60} turned into M-C_{60} upon cooling. The behavior of 1B1D phase after cooling at 100 K is similar to the 2B1D phase, see Fig. 2(b). The height differences between the B-, D-, and F-C_{60} species of the 1B1D phase (section LL′) are shown in Fig. 2(d). The height difference between the B-C_{60} and the D-C_{60} is still $\sim 0.9 \pm 0.1$ Å, and between B-C_{60} and M-C_{60} is $\sim 0.3 \pm 0.1$ Å [Fig. 2(d)]. All the above-quoted bright-and-dim height differences are likely of topographic nature. It is now accepted that C_{60} in different orientations can give slight height difference (~0.2 Å or less) in topographic STM images. For larger height difference (~0.5 Å or above), it indicates the presence or difference of interface reconstruction.[23] In addition, all observed height differences were nearly bias independent, supporting the C_{60} contrast as of topographic origin. This suggests that the B-, D-, and F-C_{60} have different adsorption interface structure but are identical in either the 2B1D or 1B1D phases. It is also noted that the bright rows of the 2B1D and 1B1D phases are often "offset," i.e., they shift sideway near the kink sites. Such a row offset is shown by the dashed lines in Figs. 2(a) and 2(b).

We further examine the ratios of B-, D-, F- and M-C_{60} of 2B1D at room temperature and 100 K [Fig. 3(a)]. Upon cooling, the B-C_{60} ratio is nearly unchanged. The disappearance of the F-C_{60} leads to increased ratios of both the D-C_{60} and M-C_{60} with about an equal probability. The ratios of the B-, D-, F- and M-C_{60} species of 1B1D at room temperature and 100 K were counted in Fig. 3(b). At 100 K, the F-C_{60} ratio reduces from 45.3% to 0%. Most of F-C_{60} molecules turn into D-C_{60}, as the D-C_{60} ratio increases markedly from 5% to 33.2% and the M-C_{60} ratio to 6.7%. As mentioned earlier, the F-C_{60} species indeed is much more abundant in the 1B1D phase and the ratios of M-C_{60} correspond to the density of kink sites. Therefore, M-C_{60} is not simply the "static" contrast of the frizzy F-C_{60}. The M-C_{60} and F-C_{60} must be considered as distinct as they are likely to have different adsorption structures.

Annealing experiments showed that both 2B1D and 1B1D are equilibrium structures. Figure 4(a) shows the evolution of the B-, D-, and F-C_{60} ratios in the 2B1D structure after annealing to different temperatures for 1 h. The statistics were measured at 300 K. The 2B1D structure remains the same up

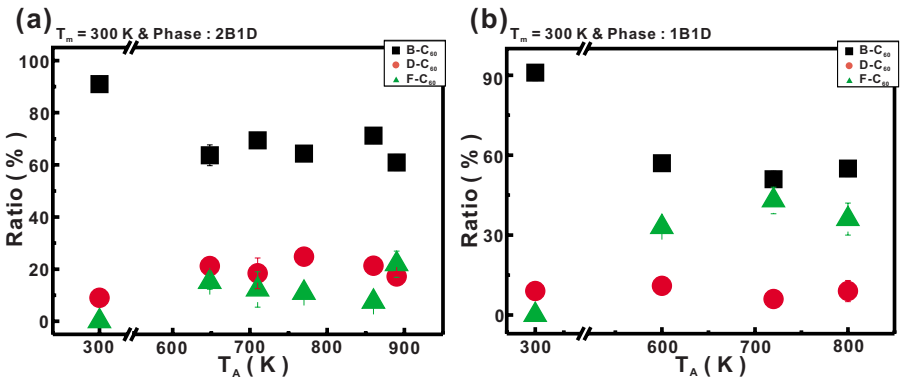

FIG. 4. (Color online) (a) and (b) show, respectively, the ratios of B-, D-, and F-C_{60} in the 2B1D and 1B1D phases with different annealing temperatures. The ratios become approximately fixed above proper temperatures.

to $T_A \sim 890$ K. At $T_A \sim 960$ K, C_{60} desorbs or decomposes, reducing the 2B1D phase coverage but otherwise leaving the surface contaminated with carbon fragments [see Fig. 5(a)]. Without annealing ($T_A = 300$ K), most C_{60} appears bright. Upon annealing to $T_A \geq 650$ K, the B-C_{60} ratio decreases, indicating thermally activated interface reconstruction similar to, e.g., C_{60}/Cu(111).[8,11] The ratios of B-, D-, and F-C_{60} reach static values and are averaged at 63.7%, 21.2%, and 15.1%, respectively, with only insignificant variation. Figure 4(b) shows the ratios of B-, D-, and F-C_{60} of 1B1D post annealed from 600 to 800 K. The ratios remain approximately fixed. Similar to the 2B1D case, at room temperature the B-C_{60} is the dominant species. The decomposition of C_{60} already occurs at a lower temperature ($\sim$880 K) as compared with the temperature $\sim$960 K for 2B1D, see Fig. 5(b). Comparing the various C_{60} ratios of the 1B1D and 2B1D superstructures, we note that the B-C_{60} and D-C_{60} ratios decrease in 1B1D but the F-C_{60} ratio increases dramatically from $\sim$10% to $\sim$40%. Since for both annealed 1B1D and 2B1D phases the ratios of B-, D-, and F-C_{60} are independent of thermal treatment if heated in the proper temperature range, it indicates that both phases are thermal equilibrium phases. We also note the quality of 2B1D and 1B1D phases improves after annealing at higher temperature. Figures 5(c) and 5(d) show the 2B1D and 1B1D phases annealed at 890 K and 800 K, respectively. Clearly, the superstructures are much better ordered when compared with Figs. 1(a) and 1(b) (annealed at 650 K and 600 K), respectively. This also suggests that the pure 2B1D and 1B1D phases are more thermodynamically stable.

The main unexpected finding is the two different superstructures at full and half ML coverage, respectively. There are quite a few other cases of coverage-dependent superstructure transitions in thin films. For example, alkali adsorption often leads to different ordering superstructures at different coverages.[24–26] In molecular films, such transitions are also known.[27–29] This is mainly due to the molecule-molecule interactions and possibly affected by molecule-substrate interactions as well. Therefore, the different superstructure phases often have varied packing density as the molecular interactions stabilize the superstructure in different ways. For C_{60} films, as observed in all other studies and the present one, strong C_{60}-C_{60} interactions simply lead to close-packed islands. While there could exist various metastable packing structures,[11] the well-annealed films often exist in one particular ordering only and it is expected *not* to observe any coverage-dependent thermal equilibrium states. Therefore, the observed 2B1D-1B1D superstructure transition appears to fall into a different category. We will offer a plausible explanation.

Thermal annealing does not drive the superstructure transition; it only stabilizes either the 2B1D and 1B1D phases as shown in Figs. 5(c) and 5(d). Instead, we consider the relevant energy terms to stabilize these two phases. As a first-order approximation, it is natural to treat the C_{60} island energy as a linear function of its size. This sole energy term clearly cannot explain the superstructure transition. Further refinement must take island boundary energy and corner energy into consideration. This has been often done, e.g., for homoepitaxial metallic islands.[30] Here for C_{60} islands with superstructure and unknown details of C_{60} adsorption geometry inside an island and at the island step, it is impossible to take a theoretical analysis much further. Instead, we give a heuristic argument, explaining that the energy of C_{60} island boundary (between C_{60} and bare Cu) drives the 2B1D-1B1D transition. At full coverage, the boundary energy is irrelevant because they are almost eliminated. For half coverage, the C_{60} island boundary length is much increased (likely to be the maximum for all coverage less than 1 ML). If the 2B1D or 1B1D C_{60} islands have distinct boundary geometry, they will have different boundary energy. We first examined whether the boundary structure is simply a truncated termination of the superstructure phase. Figure 6(a) shows the boundary structure of the 1B1D phase. Interestingly, along the C_{60} $[1\bar{1}0]$ row direction (P) we found in all cases the islands are terminated with a bright C_{60} row instead of the expected 1:1 stoichastic B:D ratio. Along the approximately orthogonal direction (P′), all terminated C_{60} molecules also appear bright. For the 2B1D phases, the coverage is nearly full and we only observed boundary structure in small vacancies as shown in Fig. 6(b). The 2B1D boundary structure is clearly more irregular. The 2B1D and 1B1D phases therefore indeed have different boundary structures. Because the 2B1D phase is the preferred phase at full coverage, the areal energy term (E_a) must be smaller. When the C_{60} overall coverage is reduced, boundary becomes present and the total energy E must include the step energy term E_b as well. For a fixed island shape with area A and boundary length L, the total energy $E = A \times E_a + L \times E_a$. To optimize E, the island shape can alter (Wulff construction[31]) or, in our case, the superstructure can change. The latter is most likely to occur when at least two superstructures are nearly degenerate in energy.

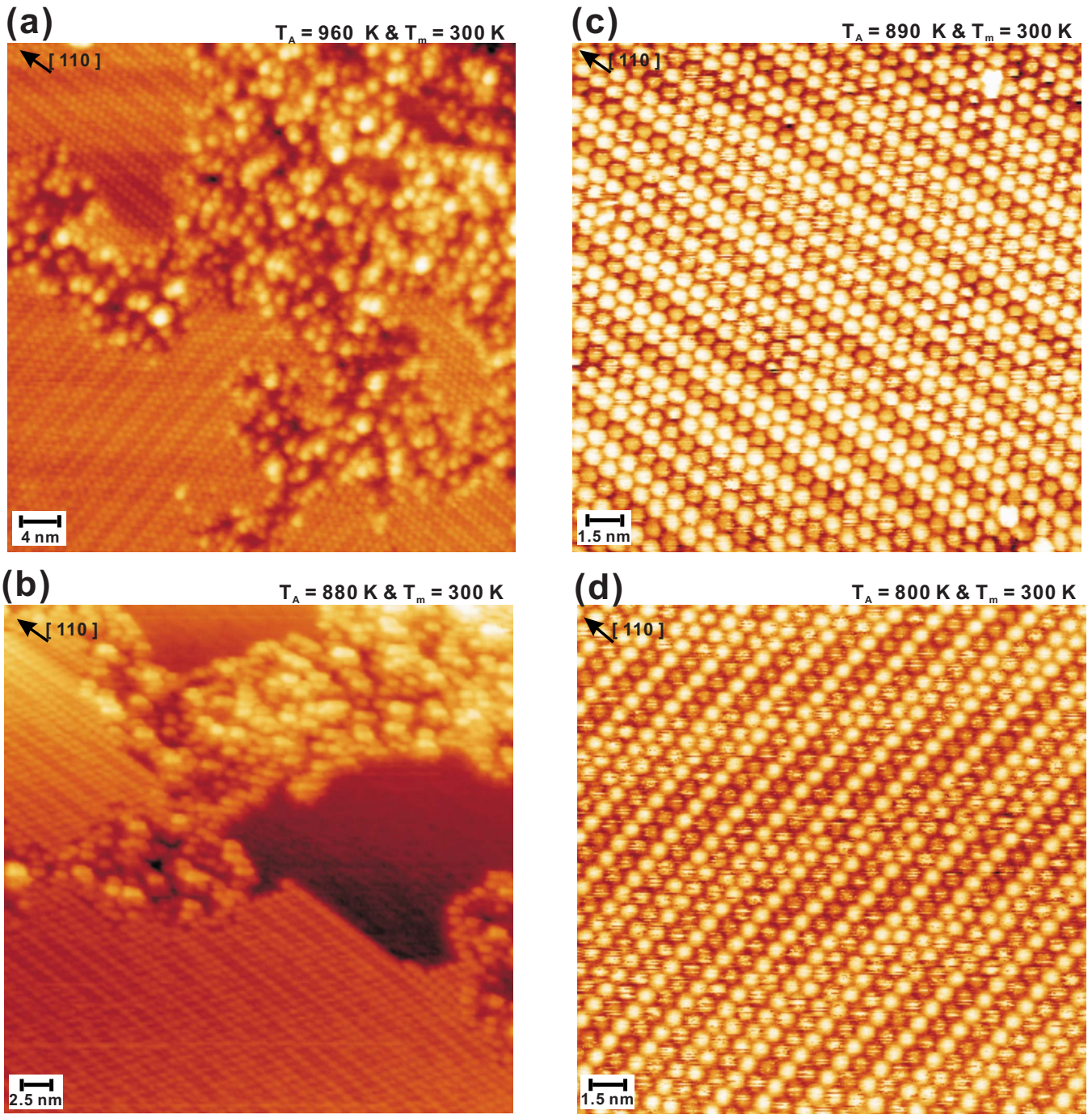

FIG. 5. (Color online) (a) At $T_A \sim 960$ K, C_{60} desorbs or decomposes in the 2B1D phase. (b) The decomposition of C_{60} was also observed in the 1B1D phase albeit with a lower $T_A \sim 880$ K. In (c) and (d), we observed that after more extensive annealing, the 2B1D and 1B1D phases become much more ordered when compared with that of Figs. 1(a) and 1(b), respectively.

We believe the 2B1D and 1B1D phases satisfy this condition. For the transition to occur, there should be a threshold "surface-volume ratio" L/A, which in terms depends on the coverage. Therefore, the presence of the lower-energy 1B1D boundary compensates the energy cost for converting the 2B1D phase to the 1B1D phase. For a surface coverage of 0.7 ML (not shown), we observed patches of area with either the 1B1D phase or a mixed 2B1D-1B1D phase. The latter appears somewhere between that of Figs. 1(a) and 1(b). This observation is also consistent with our heuristic argument because different C_{60} islands have different L/A ratios and thus may stabilize at different superstructures. For 0.5 ML, the predominant superstructure is 1B1D, in particular, after sufficient annealing. Because our argument is heuristic, we have omitted other subtle factors such as island corner energy and C_{60} domain boundary.

Finally, we comment on the observed thermal stability of the 1B1D and 2B1D phases. There have been many studies for C_{60} adsorption on metal surfaces, with film desorption temperatures reported in some cases, e.g., Ni(110)

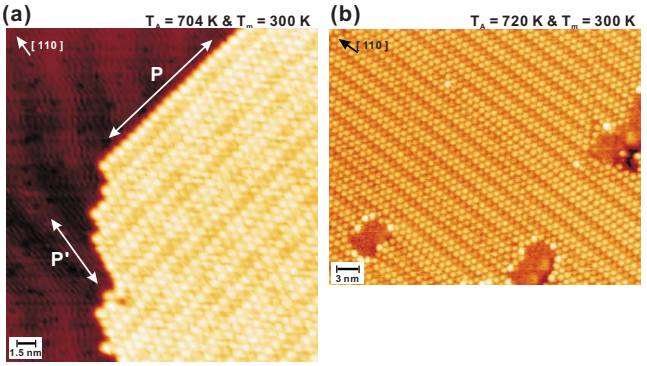

FIG. 6. (Color online) P and P′ in (a) show the directions and boundary structure of the 1B1D phase. Along the P edge, the islands are exclusively terminated with bright C_{60} rows. Along the P′ edge, all terminated C_{60} also appears bright. For the 2B1D phase in (b), the boundary structure is more irregular.

(~760 K),[32] Pt(111) (~560 K),[32] Cu(110) (~730 K),[9] Au(111) (~773 K),[33] and Ag(111) (~773 K).[32,33] These desorption temperatures are all lower than what was observed in C_{60}/Cu(001), e.g., 880–960 K. A recent study[8,11] has shown that C_{60} induces extensive reconstruction on Cu(111). For C_{60} on Cu(001), the bonding could also be strong and lead to a high desorption or decomposition temperature. For the frizzy appearance of F-C_{60}, it could due to fast C_{60} rotation. Altman *et al.*[34] have reported contrast switching from bright C_{60} to dim C_{60} and vice versa on Au(111) and attributed it to C_{60} rotation. There exists another scenario, i.e., a C_{60} can also reside in a "dynamic" adsorption geometry that changes due to short-range substrate mass flow. This was observed in the C_{60}/Ag(100) system[18] in which the contrasts of three different species (B-, M-, and D-C_{60}) can switch at room temperature. Local microscopic detailed balance was established, indicating short-range mass transport. Since we argue that the F-C_{60} and D-C_{60} are more alike [Fig. 4(b)] but the topographic height between the F-C_{60} and D-C_{60} is ~0.5 Å, it appears unlikely that this is purely due to different C_{60} orientations. Instead, a short-range mass flow changes the Cu structure beneath C_{60}, with possibly a concomitant change in C_{60} orientation, is more likely. In contrast to C_{60}/Ag(100), the much faster contrast switching rate seen here is related to a more facile adsorption structure through adding or extracting Cu atoms below the F-C_{60} species. Upon cooling, even a short-range substrate mass transport is quenched, explaining why the frizzy F-C_{60} disappears. We surmise that the facile nature of F-C_{60} may initiate the transition between 2B1D and 1B1D.

In summary, we have studied a coverage-dependent superstructure transition of C_{60}/Cu(001) by STM at room temperature and 100 K. For a coverage of 0.5 ML, C_{60} orders in an 1B1D row sequence whereas for an one ML C_{60} film the preferred ordering is a 2B1D sequence. We give a heuristic argument that the transition is driven by C_{60} island boundary energy. A fast-contrast-switching C_{60} species (F-C_{60}) and the high thermal film stability were also characterized. Our study shows that C_{60} adsorption on a substrate with an incommensurate symmetry and lattice can lead to a variety of complicated adsorption phenomena. Furthermore, the previously unknown coverage-dependent superstructures of a C_{60} film may offer a possibility to make functional molecular thin films.

This work was supported in part by the National Science Council of Taiwan through Grants No. NSC 95-2120-M-002-015, No. NSC 95-2112-M-002-051-MY3, and No. NSC 98-2112-M-002-013-MY3.

*wpai@ntu.edu.tw
†mtlin@phys.ntu.edu.tw

[1] H. W. Kroto, J. R. Heath, S. C. O'brien, R. F. Curl, and R. E. Smalley, Nature (London) **318**, 162 (1985).
[2] R. J. Wilson, G. Meijer, D. S. Bethune, R. D. Johnson, D. D. Chamblis, M. D. de Vries, H. E. Hunziker, and H. R. Wendt, Nature (London) **348**, 621 (1990).
[3] Y. Z. Li, J. C. Patrin, M. Chander, J. H. Weaver, L. P. F. Chibante, and R. E. Smalley, Science **252**, 547 (1991); **253**, 429 (1991).
[4] Y. Z. Li, M. Chander, J. C. Patrin, J. H. Weaver, L. P. F. Chibante, and R. E. Smalley, Phys. Rev. B **45**, 13837 (1992).
[5] T. Hashizume, K. Motai, X. D. Wang, H. Shinohara, Y. Saito, Y. Maruyama, K. Ohno, Y. Kawazoe, Y. Nishina, H. W. Pickering, Y. Kuk, and T. Sakurai, Phys. Rev. Lett. **71**, 2959 (1993).
[6] Y. Kuk, D. K. Kim, Y. D. Suh, K. H. Park, H. P. Noh, S. J. Oh, and S. K. Kim, Phys. Rev. Lett. **70**, 1948 (1993).
[7] E. I. Altman and R. J. Colton, Phys. Rev. B **48**, 18244 (1993).
[8] W. W. Pai, H. T. Jeng, C.-M. Cheng, C.-H. Lin, X. Xiao, A. Zhao, X. Zhang, G. Xu, X. Q. Shi, M. A. Van Hove, C.-S. Hsue, and K.-D. Tsuei, Phys. Rev. Lett. **104**, 036103 (2010).
[9] P. W. Murray, M. Ø. Pedersen, E. Lægsgaard, I. Stensgaard, and F. Besenbacher, Phys. Rev. B **55**, 9360 (1997).
[10] W. W. Pai, C.-L. Hsu, C. R. Chiang, Y. Chang, and K. C. Lin, Surf. Sci. **519**, L605 (2002).
[11] W. W. Pai, C.-L. Hsu, M. C. Lin, K. C. Lin, and T. B. Tang, Phys. Rev. B **69**, 125405 (2004).
[12] J. K. Gimzewski, S. Modesti, and R. R. Schlittler, Phys. Rev. Lett. **72**, 1036 (1994).
[13] J. Weckesser, C. Cepek, R. Fasel, J. V. Barth, F. Baumberger, T. Greber, and K. Kern, J. Chem. Phys. **115**, 9001 (2001).
[14] J. Weckesser, J. V. Barth, and K. Kern, Phys. Rev. B **64**, 161403 (2001).
[15] A. J. Maxwell, P. A. Brühwiler, D. Arvanitis, J. Hasselström, M. K.-J. Johansson, and N. Mårtensson, Phys. Rev. B **57**, 7312 (1998).
[16] W. W. Pai and C.-L. Hsu, Phys. Rev. B **68**, 121403(R) (2003).
[17] X. Zhang, W. He, A. Zhao, H. Li, L. Chen, W. W. Pai, J. Hou, M. M. T. Loy, J. Yang, and X. Xiao, Phys. Rev. B **75**, 235444 (2007).
[18] C.-L. Hsu and W. W. Pai, Phys. Rev. B **68**, 245414 (2003).
[19] M. Abel, A. Dmitriev, R. Fasel, N. Lin, J. V. Barth, and K. Kern,

Phys. Rev. B **67**, 245407 (2003).
[20] N. Néel, J. Kröger, L. Limot, T. Frederiksen, M. Brandbyge, and R. Berndt, Phys. Rev. Lett. **98**, 065502 (2007).
[21] N. Néel, J. Kröger, L. Limot, and R. Berndt, Nano Lett. **8**, 1291 (2008).
[22] W. W. Pai and J. E. Reutt-Robey, Phys. Rev. B **53**, 15997 (1996).
[23] W. W. Pai, C. L. Hsu, K. C. Lin, L. Y. Sin, and T. B. Tang, Appl. Surf. Sci. **241**, 194 (2005).
[24] W. Ernst, C. Tegenkamp, H. Pfnür, K.-L. Jonas, V. von Oeynhausen, and K. H. Meiwes-Broer, Surf. Sci. **540**, 303 (2003).
[25] Z. Y. Li, K. M. Hock, and R. E. Palmer, Phys. Rev. Lett. **67**, 1562 (1991).
[26] Z. P. Hu, N. J. Wu, and A. Ignatiev, Phys. Rev. B **33**, 7683 (1986).
[27] C. Stadler, S. Hansen, I. Kröger, C. Kumpf, and E. Umbach, Nat. Phys. **5**, 153 (2009).
[28] Z. H. Cheng, L. Gao, Z. T. Deng, N. Jiang, Q. Liu, D. X. Shi, S. X. Du, H. M. Guo, and H.-J. Gao, J. Phys. Chem. C **111**, 9240 (2007).
[29] G. E. Poirier and E. D. Pylant, Science **272**, 1145 (1996).
[30] Z. Zhang and M. G. Lagally, Science **276**, 377 (1997).
[31] G. Wulff, Z. Kristallogr. **34**, 449 (1901).
[32] M. Pedio, K. Hevesi, N. Zema, M. Capozi, P. Perfetti, R. Gouttebaron, J.-J. Pireaux, R. Caudano, and P. Rudolf, Surf. Sci. **437**, 249 (1999).
[33] E. I. Altman and R. J. Colton, Surf. Sci. **295**, 13 (1993).
[34] E. I. Altman and R. J. Colton, in *Atomic and Nanoscale Modification of Materials: Fundamentals and Applications*, NATO Advanced Study Institute, Series E: Applied Sciences Vol. E239, edited by P. Avouris (Plenum, New York, 1993), p. 303.